Chemical and conformational control of the energy gaps involved in the thermally activated delayed fluorescence mechanism

Paloma L. dos Santos, Marc K. Etherington and Andrew P. Monkman

This review summarises the significant developments in our understanding and control of thermally-activated delayed fluorescence (TADF) molecules and the spin-vibronic coupling mechanism, from which we have designed new generations of emitters. It covers both the theoretical and experimental characterization of the physical and chemical aspects of model TADF emitters. We focus on how to correctly obtain the singlet-triplet energy gaps (ΔE_{ST}) that must be overcome by the triplet excited states in the reverse intersystem crossing (rISC) process, highlighting the differences between: the ΔE_{ST} estimated from the energy difference between the fluorescence and phosphorescence (^{1}CT-^{3}LE gap); and the activation energy (Ea) estimated from the Arrhenius plot (^{1}CT-^{3}CT gap). The discussion considers the different external factors and design principles that can influence these energy gaps and ultimately the device performance.

1. Introduction

The first report on delayed fluorescence (DF) was made by *Perrin*[1] in 1929, who observed two long-lived emissions, naming them phosphorescence and fluorescence of long duration. DF was further studied in more detail by *Magel et al.*[2] (1941), *Hatchard et al*.[3] (1961) and *Horrocks et al.*[4] (1968) in fluorescein, eosin and aromatic hydrocarbons, respectively. *Wilkinson* termed this E(osin)-type fluorescence as thermally-activated delayed fluorescence (TADF)[5].

In 1996, *Berberan-Santos et al.*[6], reported DF in fullerene derivatives, and later derived rate equations[7] to describe the time-resolved processes of the DF mechanism. TADF remained a typical scientific curiosity until 2009 when *Adachi et al.* achieved a breakthrough in harnessing the mechanism to generate DF in organic light emitting diodes (OLEDs)[8]. They observed that TADF was harvesting non-emissive triplet excited states in Sn^{4+}–porphyrin devices due to the small energy splitting between singlet and triplet states observed in these compounds. Following this idea, the first TADF-based OLED without heavy-metals was reported in 2012[9]. Since then, the TADF mechanism has attracted considerable interest, mainly in the electroluminescence field, leading to OLEDs with high performance[10–13], promising a revolution in the smartphone and flat panel displays industry.

The TADF mechanism (i, **Fig.1**) can up-convert 100%[14] of the lower energy triplet excitons (dark states) into higher energy emissive singlet states by reverse intersystem crossing (rISC), thereby surpassing the 25% internal quantum efficiency (IQE) in OLEDs imposed by spin statistics[15]. However, there are two other mechanisms that have the ability to harvest triplet states using metal-free organic molecules: ii) triplet-triplet annihilation (TTA) and iii) upper triplet crossing, also called "hot-exciton". **Figure 1** shows a diagram comparing all three mechanisms.

TTA (ii, **Fig.1**) is a bimolecular process that occurs between two colliding triplet states forming an encounter complex which can have singlet, triplet or quintet character. If the resulting excited state is a singlet, the most desirable outcome, the TTA mechanism can result in DF and certainly increase the OLED performance[16–19]. However, within the best possible alignment of energy levels, TTA can only achieve IQE values up to 62.5%[20], whereas TADF can result in IQEs of 100%. Another strategy to up-convert dark states is called "hot exciton" (iii, **Fig.1**), which is a rISC process from upper excited singlet and triplet levels (S_n,T_n), followed by internal conversion (^{1}IC) to the lowest singlet states and then recombination to the ground state through the emission of photons. Such upper state rISC was reported in several well-known dyes such as rose Bengal and erythrosin B[21,22]. More recently, *Hu et al.*[23] rediscovered this mechanism. Thus, 100% of the triplets formed from charge recombination can, initially, be converted into emissive singlet states. However, the internal conversion (IC) between triplet states T_n and T_1, ^{3}IC, needs to be suppressed to ensure a larger production of singlet states and, in most of the organic molecules IC is very efficient, making it difficult to achieve efficient rISC to out compete ^{3}IC[24]. Thus, this mechanism as an

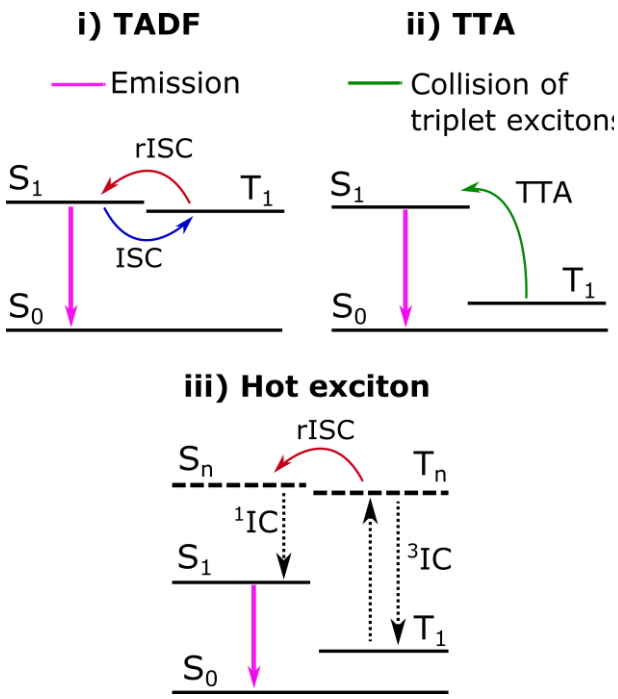

Figure 1 Simplified schematic representation of the electronic energy levels involved in i. Thermally-activated delayed fluorescence (TADF) ii. Triplet-triplet annihilation (TTA) and the iii. Hot exciton mechanism.

approach to increasing the OLED performance has not yet shown significant merits. TADF, therefore, is the most promising and efficient mechanism to convert triplet states to singlet states, and it is currently the most intensively studied area of OLEDs.

Two well-known challenges for TADF emitters concerning OLED performance are: efficiency roll-off with increasing current to attain high brightness; and moderate external quantum efficiency (EQE) values. Many of the TADF emitters show higher roll-off and lower EQE than those observed in devices based on phosphorescence emission (PH-OLEDs)[25], which contain costly heavy elements such as Ir and Pt. Major challenges also persist concerning the full understanding of the mechanism, mainly the rISC process, which has a rate strongly affected by the environment in which the emitter is dispersed, the regio-isomerization of the molecules and the different conformations that the molecules can access.

To help understand the TADF mechanism, this review covers both the theory and experimental characterization of the physical and chemical aspects that are relevant in the development of new TADF molecules for high efficiency OLEDs. In particular, it focuses on how to obtain the correct singlet-triplet energy gaps (ΔE_{ST}) that must be overcome by the triplet excited states in the rISC process as highlighted by the spin-vibronic coupling mechanism[26] and the need for three excited states to come into resonance to achieve high TADF efficiency[27–29]. Practical challenges of high efficiency OLEDs, e.g. outcoupling, can be found in a recent review paper by *Gather and Reineke*[30].

2. Fundamental understanding of the TADF mechanism

Figure 2a shows the fundamental energy levels and the rate constants involved in the TADF mechanism to generate photoluminescence. For many donor-acceptor (D-A) and donor-acceptor-donor (D-A-D) type TADF molecules there are two possible excitation channels. Firstly, the molecules may be excited via a strong local D (or A) π-π*transition, which forms a locally excited singlet state (^{1}LE). Following this, the excitation can either undergo electron transfer (ET) to form a CT state, radiative decay to the ground state or intersystem crossing (ISC) to the locally excited triplet states, ^{3}LE. Secondly, they may be excited via a weak n-π* transition directly generating the ^{1}CT state[28]. The former is the more usual experimental situation, thus, following photoexcitation (absorption), depending on the rate of ET it is possible to detect ^{1}LE emission in the first few nanoseconds of decay, but the majority of excitations are transferred to the ^{1}CT manifold by very slow (of order 10^8 s^{-1}) ET. This ET is slow because of the decoupling between D and A units caused by near orthogonality between them even in the ground state (due to the N-C bridging bond). Once the ^{1}CT is formed, three distinct processes followed: i. radiative emission yielding prompt ^{1}CT fluorescence (PF), a fast decay component (nanosecond range) with rate constant assigned as K_{PF}; ii. non-radiative decay, $^1K_{nr}$; or iii. intersystem crossing (ISC) to the CT triplet states, followed by relaxation to the lowest energy triplet state. Once the triplet states are reached, they can either recombine to the ground state by radiative (K_{PH}) or non-radiative emissions ($^3K_{nr}$), or (spin) flip back to the singlet state (K_{rISC}). Normally it is assumed that the latter process just requires thermal energy to raise the triplet state to a vibronic sub-level that is isoenergetic with the emissive singlet states to enable reverse intersystem crossing (rISC) because spin flip is an adiabatic process. These final emissive singlet states emit in the microsecond to millisecond regime due to the involvement of the longer-lived triplet states. This means that the thermally-activated delayed fluorescence that occurs as a result of rISC is sensitive to heat and oxygen. For TADF to occur, the energy splitting between singlet and triplet states, ΔE_{ST}, should be very small (less than a few hundreds of meV but ideally less than a few tens of meV for efficient rISC) only then can most of the triplet states be up-converted back to the singlet states i.e. $K_{rISC} >> K_{PH} + {}^3K_{nr}$. A detailed description of the rate constants and quantum yields involved in the TADF mechanism can be found in references[31,32]. The most common strategy in the design of TADF emitters to achieve a suitably small ΔE_{ST} is to minimize the electron exchange energy in the excited state. The predominant way to achieve this so far is in donor-acceptor (D-A) charge transfer molecules. In these D-A materials excited states with strong charge-transfer character (CT) readily form[33]. If the bridging bond between the D and A units tends to take a perpendicular steric conformation, typically the case with a N-C bridging bond[34], the interaction between the electron on the D

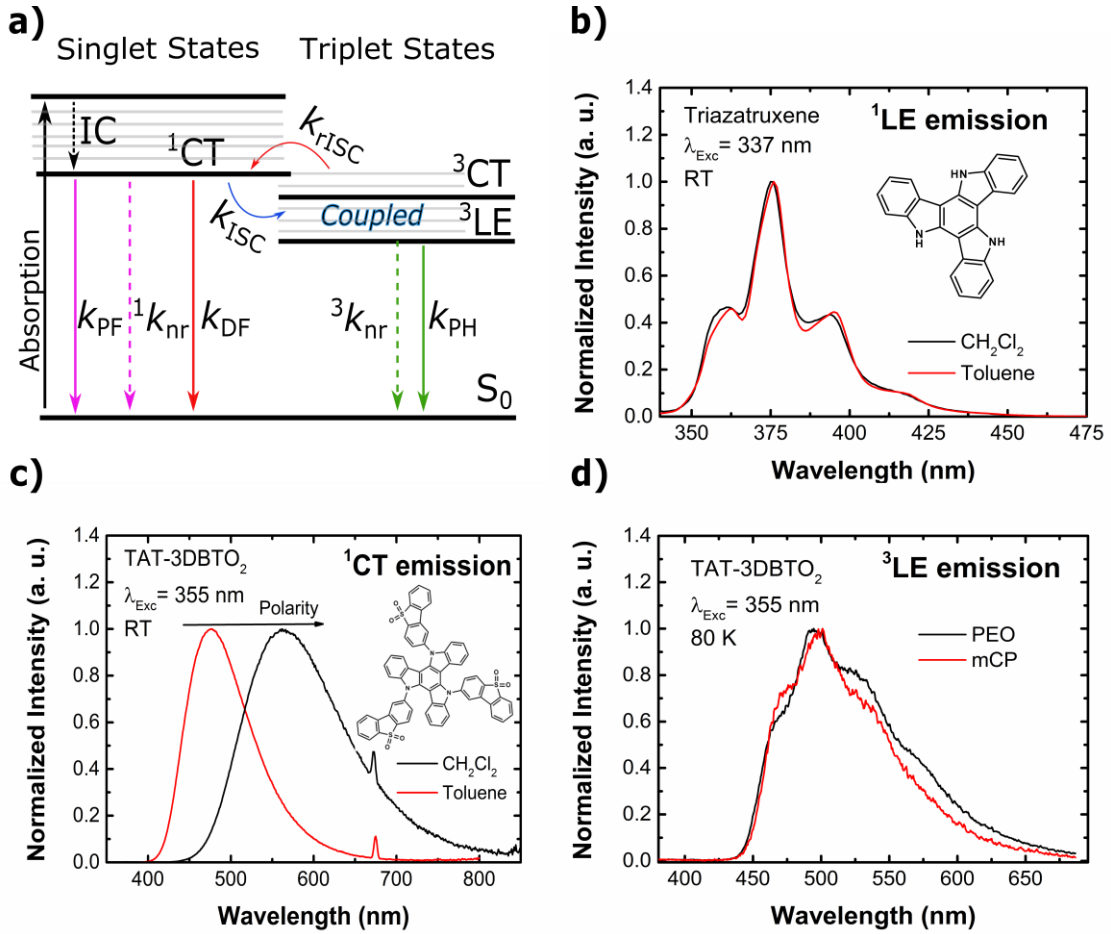

Figure 2 a) Schematic representation of the electronic and vibronic energy levels, and rate constants involved in the TADF kinetic mechanism. b) Photoluminescence spectra of Triatruxene in dichloroomethane (CH_2Cl_2) and toluene solutions. c) Photoluminescence spectra of TAT-3DBTO2 in dichloromethane (CH_2Cl_2) and toluene solutions d) Phosphorescence spectra of Triatruxene in polyethylene oxide (PEO) and N,N'-Dicarbazolyl-3,5-benzene (mCP) matrixes.

and electron on the A in the excited state is minimised giving near zero exchange energy and thus small ΔE_{ST}. Critically however, in this configuration the charge transfer singlet (CT^1) and triplet (CT^3) orbitals are degenerate and spin orbit coupling is forbidden[35]. *Monkman et al.* pointed out that this also implies that rISC is forbidden for the same reason[28]. This is why it is also a necessary requirement for efficient TADF that one of the locally excited triplet states (^{3}LE) of the D or A units mediates the spin flip mechanism via vibronic coupling to the CT states. This makes it essential to be able to differentiate between CT and LE states. CT states are very sensitive to the environment, because of their dipole moment, and the usual experimental technique used to identify CT states is to measure the solvatochromic shift of their emission spectra. The pronounced spectral shift with increasing solvent polarity is mainly due to the shielding of the excited state dipole of the TADF molecules, by rearrangement of the solvent shell around the molecule, this reduces the coulomb energy of the CT causing a red shift. As previously shown, this effect saturates when the CT state becomes fully relaxed. Occasionally, on freezing, the solvent shell can no longer reorient to relax the coulomb energy and dramatic blue shift of the CT emission accompanies the freezing of the solvent shell[36]. LE states, on the other hand, are insensitive to changes in the environmental polarity. **Figure 2b** gives an example of the locally excited singlet state (^{1}LE) of an electron donor unit, triazatruxene (molecular structure in the inset of the graph). As can be seen, the emission spectra is not influenced by changing the polarity of the environment. However, the ^{1}CT emission of TAT-3DBTO$_2$ (**Fig. 2c**), molecules formed when a triazatruxene core is attached to three dibenzothiophene-*S,S*-dioxide acceptor units, shows strong solvatochromism[37]. The ^{1}CT emission has onset at (2.97 ± 0.02) eV in toluene and (2.63 ± 0.02) eV in dichloromethane. Another experimental observable to differentiate ^{1}LE and ^{1}CT states, arises from the fact that the ^{1}LE emission spectra usually have well-resolved vibronic structure whereas the ^{1}CT are structureless and Gaussian-like. Similar analyses can be translated to the triplet states, i.e., the ^{3}LE are almost unaffected by the polarity of the environment (**Fig. 2d**). The PH spectrum of TAT-3DBTO$_2$ films was investigated in two media, a polymer (polyethylene oxide, PEO), and a well-known host compound (N,N'-Dicarbazolyl-3,5-benzene, mCP). In both films,

the PH spectrum shows vibronically structured ^{3}LE character from the acceptor units and same onset energy value in both polar and non-polar environment. This ^{3}LE energy, combined with ^{1}CT, is used to calculate the 'optical' ΔE_{ST}. Emission from ^{3}CT states has not yet been identified experimentally in our work, which includes a vast range of efficient TADF emitters[28,38,39]. This can be associated to a few different factors, most obviously, the small energy gap between ^{1}CT-^{3}CT makes them difficult to distinguish and the oscillator strength of CT states is already weak for the singlet state and this would be further compounded by the forbidden nature of triplet decay. Due to these difficulties extra caution should be applied when analysing the phosphorescence of TADF molecules to ensure identification of the correct state. Once the singlet and triplet states are measured in the TADF emitters, it is still not a simple task to determine those involved in the TADF (singlet-triplet) energy gap, ΔE_{ST}. In many materials, the onset of fluorescence and phosphorescence emission are difficult to estimate and in D-A molecules the phosphorescence spectra may be a superposition of both the donor and acceptor ^{3}LE phosphorescence. The need to deconvolute the energies of the two local phosphorescent states was shown in recent work by our group[28], which allowed the correct energy gap between the ^{1}CT fluorescence and the lowest energy donor ^{3}LE phosphorescence to be obtained. A further complication that is often found is that the optical ΔE_{ST} is different to the thermal activation energy calculated from the rISC rate, k_{rISC}, using **equation 1**:

$$k_{rISC} = A\, e^{\frac{-E_a}{RT}} \quad (1)$$

where A is a pre-exponential factor, E_a is the activation energy for the rISC process, R is the gas constant and T is temperature. It is not just the initial and final states, ^{1}CT and ^{3}LE, that are crucial to the rISC rate, but also an intermediate mediator state is required, which defines more than one ΔE_{ST} as discussed below.

Spin orbit coupling (SOC) is formally forbidden between singlet and triplet CT states for the case of near orthogonal D and A units where the exchange energy approaches zero[35], and thus other electronic states must be involved in the rISC mechanism to mediate the spin-orbit coupling spin flip. We have shown that the energetically nearest ^{3}LE state plays an important role in the ΔE_{ST} [28,29,39] , however, just the SOC between ^{3}LE and ^{1}CT is still not able to explain the high rates of rISC reported experimentally.

Ogiwara et al. [40] proposed an alternative mechanism from electron paramagnetic resonance (EPR) spectroscopy to probe the population of the ^{3}LE and ^{3}CT states. They observed an EPR signal consistent with the mixture of both ^{3}LE and ^{3}CT states, concluding that efficient rISC not only includes the SOC pathway (^{3}LE→^{1}CT), but also a hyperfine coupling (HFC) induced ISC pathway (^{3}CT→^{1}CT). Recently, *Gibson et al*. [26] have shown that neither of these processes explain the measured TADF spin flip rate >10^6 s^{-1}. By utilising a more rigorous quantum dynamics approach to describe the K_{rISC} that considers the vibrational density of states and implementing second-order perturbation theory they demonstrate that both ^{3}CT and ^{3}LE are pivotal to the rISC process. From this it has been identified that there are at least two energy gaps to consider when optimizing TADF molecules. TADF uses thermal energy to vibronically couple (mix) the ^{3}LE and ^{3}CT triplet states to achieve a thermal equilibration between the states (akin to reverse internal conversion) and once in this coupled state adiabatic SOC can occur between the ^{3}CT and ^{1}CT states mediated by the ^{3}LE state (see **Fig. 2a**). With consideration of vibronic coupling the rISC rate can then be defined as **equation 2**, according to second-order perturbation theory

$$\mathbf{k_{rISC}} = \frac{2\pi}{\hbar}\left|\frac{\langle {}^1\boldsymbol{\psi}_{CT}|\hat{\mathbf{H}}_{SOC}|{}^3\boldsymbol{\psi}_{LE}\rangle\langle {}^3\boldsymbol{\psi}_{LE}|\hat{\mathbf{H}}_{vib}|{}^3\boldsymbol{\psi}_{CT}\rangle}{\boldsymbol{\delta}({}^3\mathbf{E}_{LE} - {}^3\mathbf{E}_{CT})}\right|^2 \boldsymbol{\delta}({}^3\mathbf{E}_{CT} - {}^1\mathbf{E}_{CT}) \quad (2)$$

The above equation takes into account the locally excited triplet state as a mediator to the rISC and TADF process. The non-adiabatic coupling between ^{3}LE and ^{3}CT reduces the activation for rISC by forming an equilibrium between these two states, even without thermal activation[41]. This lowering of the energy gap occurs because, according to the second-order perturbation theory, E_a is dominated by the ^{1}CT-^{3}CT energy gap rather than the ^{1}CT-^{3}LE energy gap. As a result, they showed the important effect of intermediate states on the E_a energy, explaining the reason for the different energy gaps associated with the TADF mechanism: the ΔE_{ST} calculated via optical energy, describes the ^{1}CT-^{3}LE gap; whereas the E_a calculated from the Arrhenius plot, describes the thermal gap between ^{1}CT-^{3}CT.

In line with these works, other theoretical study[42] also characterized the nature of the states involved in the rISC process. They showed that these electronic states are comprised of a mixture of LE and CT state contributions that vary with chemical structure and dynamically evolve following the changes in the molecular conformation and local dielectric environment, aspects discussed in detail in the following sections.

3. Design principles of TADF molecules

When designing TADF molecules it is important to ensure two conditions: i. a small energy gap between the singlet and triplet states, ^{1}CT, ^{3}CT and ^{3}LE (ΔE_{ST}), to maximize the rISC process and ii. suppression of the internal conversion pathways available for the singlet and triplet excited states, to maximize emission yields. Condition i occurs by minimization of the exchange electron energy, J, and has been extensively studied in D-A and D-A-D type molecules. These molecules show excited states with strong CT character and very small overlap between the HOMO and LUMO frontier orbitals due to spatial separation, see **equation 3**:

$$J = \iint \Phi(1)\Psi(2)\left(\frac{e^2}{r_1 - r_2}\right)\Phi(2)\Psi(1)dr_1 dr_2 \quad (3)$$

where ϕ and ψ represent the HOMO and LUMO wave-functions, respectively, and *e* is the electron charge. However, characteristic ii is not a straightforward task, and minimizing IC to obtain a strong fluorescence yield in molecules with strong CT character has been a challenge. The desired molecule should have a photoluminescence quantum yield close to 1 with a short emissive state lifetime; this is to ensure harvested triplets do not cycle back to the triplet state and to avoid decay by non-radiative pathways. This requires strong coupling of the ^{1}CT to the ground state. However, to ensure a very small ^{1}CT–^{3}CT energy gap (which is a requirement for efficient rISC), D-A orthogonality is required which effectively decouples the ^{1}CT states from the ground state. Solving this seemingly paradoxical situation is not yet fully understood, but with TAT-3DBTO$_2$, we have achieved the seemingly impossible, a rISC rate > 10^7 s^{-1} whilst retaining a PLQY ~ 1 through near degenerate multiple excited states arising from the multi D-A structure. This new emitter yields OLEDs with better performance than Ir emitter based systems including high performance at very high brightness levels, see ref [37] for full details. This new material points the way ahead for new TADF emitter design.

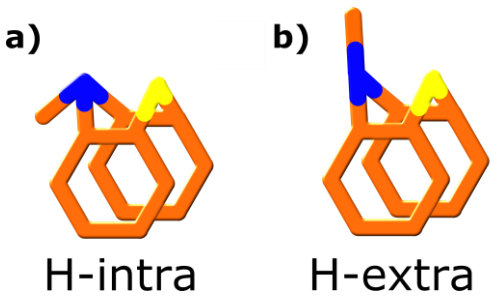

Figure 3 The two different conformers that can be obtained by phenothiazine. a) The H-intra conformation has greater delocalisation of the lone pair nitrogens into the phenyl rings of the phenothiazine, whereas b) the H-extra conformation inhibits this. The blue bonds represent nitrogen and yellow bonds sulphur. Figure adapted from reference [46].

4. Conformational Heterogeneity in TADF molecules

A further consideration is the possibility of different conformations for the D-A structures. Different conformers have different emissive states, and consequently different ΔE_{ST} and one simple way of identifying the presence of two different conformations on the same molecule is the observation of dual emission. Dual emission is commonly observed in organic molecules for the case where one emission involves the locally excited states and the other comes from CT states.

For the specific case of the phenothiazine donor, this emission dependence on conformation was first observed in 2001 by *Daub et al.*[43] in phenothiazine-pyrene dyads. Where the conformation of the phenothiazine was crucial to the energy level arrangement in the molecule thus allowing dual emission

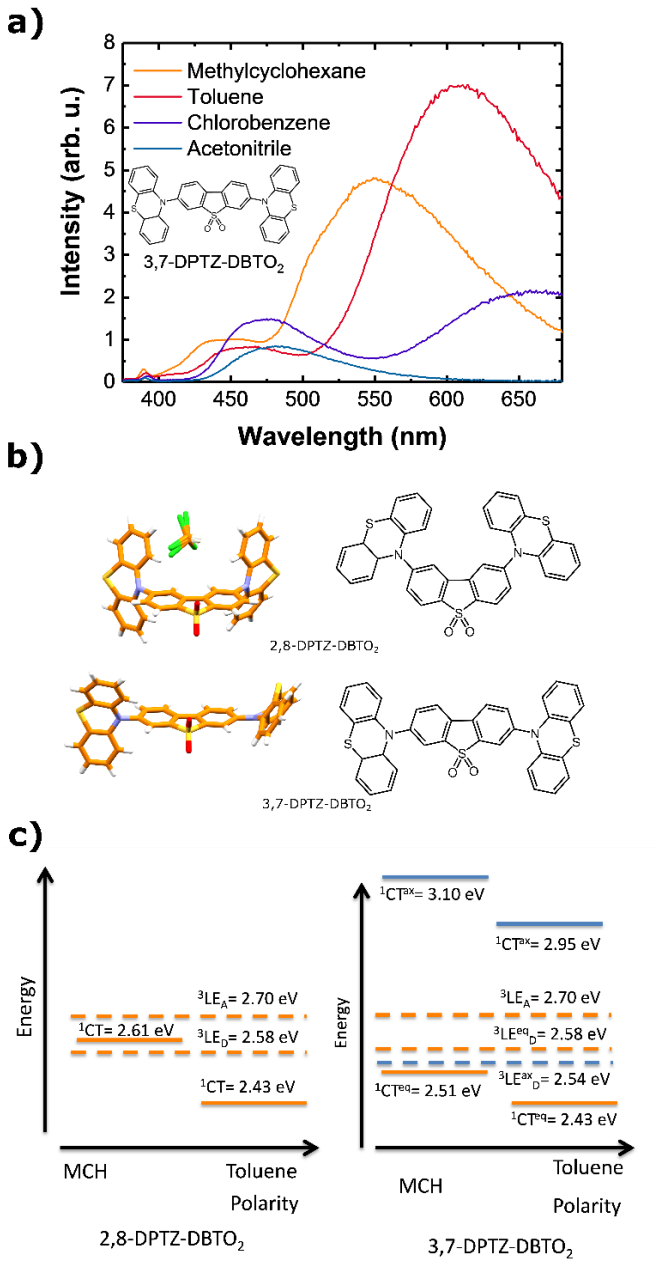

Figure 4 a) Solvatochromism of 3,7-DPTZ-DBTO_2 showing how the emissive CT states undergo a bathochromic shift with increasing solvent polarity, as a result of their larger dipole moment compared to the locally excited states. The higher energy CT emission arises from the quasi-axial conformation, a result of H-extra phenothiazine. The lower-lying CT arises from the H-intra phenothiazine, which produces a quasi-equatorial conformation. b) The crystal structures of the two regioisomers showing the two conformations of phenothiazine alongside their chemical structures c) The energy level arrangement of the two molecules showing the differences between the quasi-axial and quasi-equatorial excited state energies. The quasi-axial CT state in the 3,7-DPTZ-DBTO$_2$ is a triplet loss pathway due to low-lying ^{3}LE$^{ax}_D$ acting as a trap state. Figures taken from reference [49].

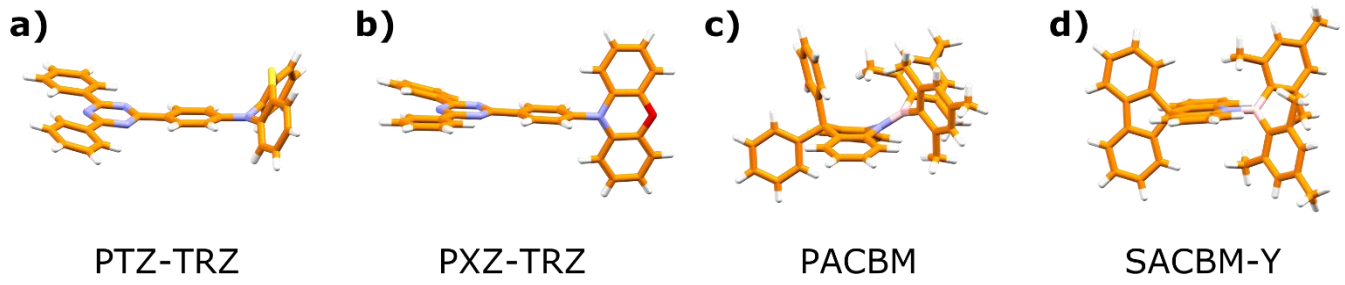

Figure 5 a) The PTZ-TRZ and b) PXZ-TRZ molecules featured in references 51 and 61, showing that the phenothiazines energetically favoured state is a quasi-axial conformation, whereas the phenoxazine is quasi-equatorial. Two of the molecules studied in reference 60 showing the quasi axial (c) and quasi-equatorial (d) behaviour is related to whether the acridine is planar (SACBM-Y) or twisted (PACBM).

of both LE and CT states. This was followed by similar observations by *Stockmann et al.*[44] in 2002 and *Acar et al.*[45] in 2003, again in phenothiazine-pyrene dyads.

To understand the origin of this dual emission in these phenothiazine-based molecules we must consider the conformational behaviour of the molecule itself. This was first discussed in the 1960s and early 1970s[46–48]. The fundamental aspect is that the phenothiazine is a distorted boat structure forming either H-intra or H-extra conformers, as shown in **Figure 3**. This leads to two different sets of electronic states; in the H-intra conformation the lone pairs of the nitrogen delocalise into the phenyl rings of the phenothiazine, which is not the case for the H-extra conformation. This ability to form H-intra and H-extra folded conformers allows formation of parallel quasi-axial and perpendicular quasi-equatorial conformations in D-A and D-A-D molecules, as will be discussed in the next section. This behaviour can be directly linked to the dual LE and CT emission observed in the early 2000s and to a more recent discovery of dual CT emission in TADF molecules leading to different ΔE_{ST}[49,50].

Adachi et al. [51] reported a D-A emitter that shows dual CT emission, PTZ-TRZ, which has phenothiazine as the donor unit and 2,4,6-triphenyl-1,3,5-triazine (TRZ) as the acceptor unit. Through density functional theory calculations, they identified the existence of two ground-state conformers that can exist with almost equal proportions in toluene solutions, named quasi-axial and quasi- equatorial. Calculations also estimated two different singlet-triplet energy gaps, 1.14 and 0.18 eV, with the latter giving rise to DF via the TADF mechanism, as confirmed by temperature dependence analyses.

Taking this into consideration the choice of donor and acceptor can have a significant impact on the final performance of the TADF D-A-D molecule in a device. Choosing a molecule that has the ability to form two different conformers can lead to unwanted emission and other possible side effects. Thus, it is desirable to find solutions to control these conformations. *Xiao-Hong Zhang et al*.[52] show this control using TADF molecules with donor units based on 9,9-dimethyl-9,10-dihydroacridine (DMAC), first reported by *Adachi et al*.[53]. The molecules have two possible conformations, which they entitled the planar and crooked forms. The dual conformations observed in 2-(9,9-dimethylacridin-10(9H)-yl) thianthrene-5,5,10,10-tetraoxide (DMAC-TTR) molecules resulted in low performance OLEDs (EQE of 13.9%), presenting a need in the development of solutions to supress the deleterious crooked form in these molecules. Thus, they presented two design strategies to address this problem: (1) increasing the rigidity of these groups to suppress the crooked form; (2) increasing the steric hindrance of the linked group to minimize the energy of the highly twisted form. Considering these two strategies, two modified TADF emitters were synthesized: (1) 2-(10H-spiro[acridine-9,9'-fluoren]-10-yl)thianthrene5,5,10,10 tetra-oxide (SADF-TTR), which has an additional fluorene group on the DMAC unit that retains a similar electron donating ability but increases the rigidity of the structure and (2)2-(9,9-dimethylacridin-10(9H)-yl)-3-phenylthianthrene-5,5,10,10te-traoxide (DMAC-PTR), which has a phenyl group attached to the ortho-position of DMAC to increase the steric hindrance between the DMAC and TTR groups. OLEDs based on these new structures exhibited a single electroluminescence peak and increased performance (EQE values of 20.2% and 18.3%), confirming the success of the strategies in controlling the dual conformations and avoiding energy loss. However, substitution on the donor (or acceptor) also has more subtle changes, including the mixing of the n-π* and π-π* states giving rise to the direct CT transition. This effects the conjugation of the D and A, the PLQY of the CT fluorescence, but not the ΔE_{ST}[54] .

Another way of avoiding dual emission is the use of rigid units, e.g. phenoxazine, which appears only display single emission as demonstrated in our recent papers[54,55]. Apart from the molecules discussed above, there exists in literature warnings for other molecules such as acridan, xanthene, thioxanthene and isoalloxazin[56,57]. Any flexible molecule should be treated with caution regarding TADF.

5. Control of ΔE_{ST} by Regio- and conformational isomerization

We recently studied two regioisomers of bis(10H-phenothiazin-10-yl)dibenzo[b,d]thiophene-S,S-dioxide D-A-D TADF emitters[49]. 2,8-bis(10H-phenothiazin-10-yl)dibenzo[b,d]thiophene-S,S-dioxide (2,8-DPTZ-DBTO$_2$) exhibits only one quasi-equatorial conformer on both donor sites, with ^{1}CT emission close to the ^{3}LE state leading to efficient TADF via spin-vibronic coupling. However, 3,7-bis(10H-phenothiazin-10-yl)dibenzo[b,d]thiophene-S,S-dioxide (3,7-DPTZ-DBTO$_2$) displays both a quasi-equatorial CT state and a

higher-energy quasi-axial CT state. The two states can be identified by investigating the solvatochromism of the molecules, with 3,7-DPTZ-$DBTO_2$ clearly showing dual CT emission in **Figure 4a**. The chemical and crystal structures of the two molecules are shown in **Figure 4b**. The mixed axial and equatorial conformations of the 3,7-DPTZ-$DBTO_2$ are readily seen in the crystal structure, and the effects of this extra conformer give rise to a doubling of the possible electronic excited states of the molecule, depicted in the energy level diagram shown in **Figure 4c**.

The presence of the low-lying ^{3}LE state of the axial conformer means that this quasi-axial CT is an effective loss pathway both photophysically and in devices and no TADF is observed in the quasi-axial CT emission as a result. However, we also find that the equatorial and axial states do not couple, so that TADF is observed if the equatorial site is excited. This raises some profound questions about conjugation and excited state coupling in strong charge transfer molecules. From measurements obtained in MCH, we observe that even though the axial local triplet is close to resonance with the equatorial CT states, the two do not couple to yield TADF, instead axial phosphorescence is the only radiative deactivation channel for the axial local triplet. In section 7 we describe how some control on the phenothiazine conformer, and thus the efficiency of TADF, in the design of the molecule can be achieved.

The possibility of two different conformations on the connecting position of the donor to acceptor is prominent in phenothiazine and other flexible (distorted) molecules. However, regioisomerisation can influence the TADF properties of a molecule without this behaviour. In recent work from *Grazulevicius*' group[58] in Lithuania, and as originally shown by *Dias and Monkman et al.*[14], the connection of a rigid donor molecule like carbazole in the para- and meta- position on a central acceptor can have a significant effect on the TADF. The difference between the para- and meta- connection affects the charge-transfer character of the molecule. The para- connected system benefited from a higher oscillator strength of the lowest energy transition and a resultant higher photoluminescence quantum yield, however the singlet-triplet gap was much higher. The meta- connected system on the other hand, had better separation of the electron and hole densities and a much stronger charge-transfer character leading to a smaller singlet-triplet splitting and more efficient TADF. In this case the position of the donor affects the amount of π-π* and n-π* mixing and as a result the charge-transfer strength of the molecule.

As such, investigation into the simple effects of the donor acceptor position is of paramount importance. Is it simply the change in steric hindrance[59], the production of a new conformer[49,51,60] or is it related more to the fundamental electron accepting and donating nature of the molecule in the different positions?

Figures 5a and 5b shows the difference between a flexible molecule like phenothiazine and the more rigid phenoxazine. The latter, phenoxazine-2,4,6-triphenyl-1,3,5-triazine (PXZ-TRZ) forms the quasi equatorial conformation when connected to the triazine however, the phenothiazine in phenothiazine-2,4,6-triphenyl-1,3,5-triazine (PTZ-TRZ), clearly forms the quasi axial, and is the reason for the dual emission mentioned earlier. In **Figures 5c and 5d** the molecules PACBM and SACBM demonstrate how the fusing of two phenyl rings via an extra bond can affect the conformation of the central acridine donor. In PACBM when the two phenyl rings are not fused the acridine unit adopts the quasi-axial conformation, however in SACBM-Y when the phenyl rings are fused the acridine is forced into the quasi-equatorial arrangement[51,60,61].

Furthermore, it is possible to design a molecule that has dual CT emission by having an antisymmetric donor-acceptor-donor structure (D-A-D'). In our recent work in collaboration with *Zhenguo Chi et al*. dual emission was observed from a molecule featuring phenothiazine and carbazole as D and D'[62], again showing that intramolecular energy transfer is suppressed in orthogonal, molecules with strong CT character. However, even on the symmetric phenothiazine molecule, depending on how the crystal was grown, dual emission due to the quasi-axial or quasi-equatorial conformation of the phenothiazine was observed[63,64]. This sensitivity to the preparation method carries with it a warning for phenothiazine-based emitters especially relating to the control of phenothiazine conformation. This means that evaporated or drop cast films may have different emissions depending on the solvent or temperature used.

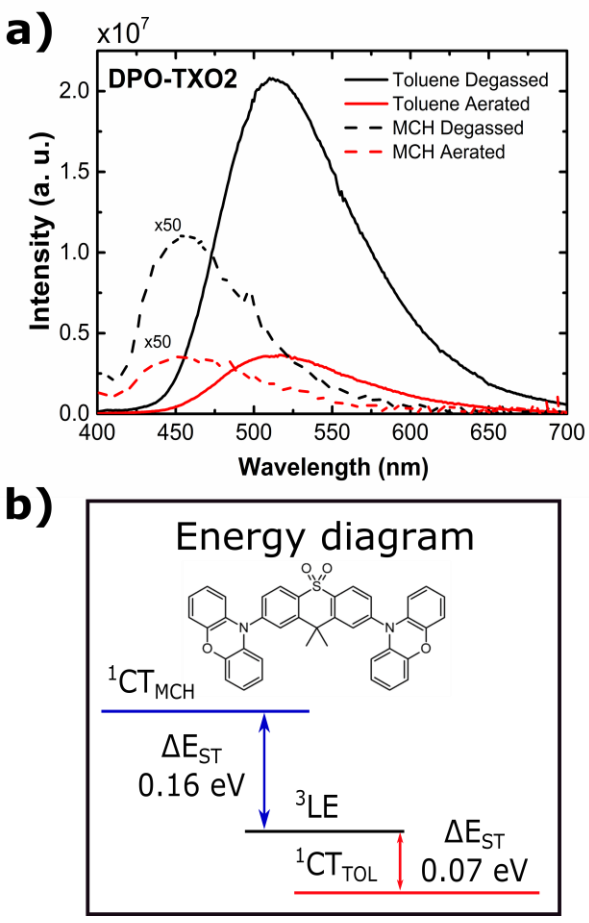

Figure 6 Photoluminescence spectra (PL) of DPO-TXO2 in methylcyclohexane (MCH) and toluene in degassed and aerated solutions. Inset graph shows the chemical structure of DPO-TXO2 and the energy level arrangement for both solutions. Figure adapted from reference [29].

6. Control of the ΔE_{ST} by changing the polarity of the environment

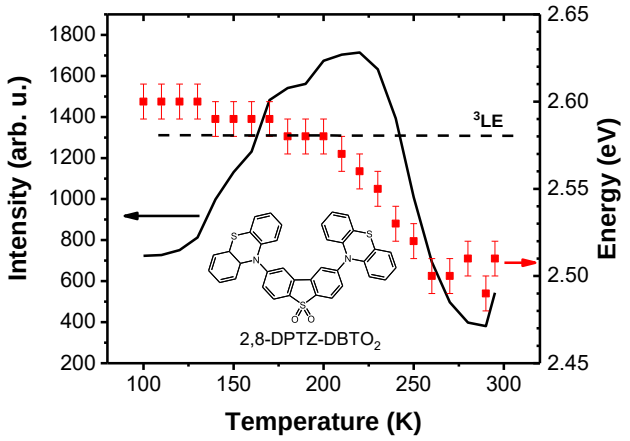

Figure 7 CT onset and Intensity change of 2,8-DPTZ-DBTO2 with temperature in a PEO host. The reduction in temperature reduces the polarity of the PEO and thus the polarity controls the CT emission and rISC rate in the system. Figure adapted from reference [27].

In the previous section we have discussed how the singlet triplet gap and thus TADF is strongly affected by regio-isomerisation and in certain cases by the creation of a second charge-transfer state. This has focused mainly on the design principles and how the molecule can be synthesised to meet these criteria. In this section we will look at how the ΔE_{ST} energy can be controlled through the polarity of the host environment.

We have demonstrated recently, that the environment can be used to control the optical ΔE_{ST} energy value, in solutions and in solid state, by studying the molecule DPO-TXO$_2$ (2,7-bis(phenoxazin-10-yl)-9,9-dimethylthioxanthene-*S,S*-dioxide), a D-A-D TADF emitter formed by phenoxazine donors and the 9,9-dimethylthioxanthene-*S,S*-dioxide (TXO$_2$) acceptor[29]. This is expected due to the fact that CT and LE states exhibit different responses to changes in the environment due to their very different polar characters, as discussed previously.

Figure 6 shows the ^{1}CT emission spectra of DPO-TXO$_2$ in methylcyclohexane (MCH) and toluene solutions. The energy difference between these two emission spectra give rise to two distinct scenarios, in MCH the ^{1}CT is located above the ^{3}LE state, and in toluene the ^{1}CT is located below the ^{3}LE. The ^{3}LE emission in DPO-TXO$_2$ comes from the donor units and its emission spectrum is shown in ref[29]. Thus, the magnitude of the ΔE_{ST} energy values for MCH and toluene were identified to be (0.16 ± 0.03) eV and (0.07 ± 0.03) eV respectively. As a direct consequence of the difference in ΔE_{ST} value the DF emission contribution to the overall emission was different in each solvent. This analysis was made by comparing the emission intensity in aerated and degassed solutions. The ^{1}CT emission increases by a factor of 3.10 (MCH) and 4.8 (toluene) when oxygen is removed (**Fig.6**). Thus, the contribution of DF is 52% and 82% for MCH and toluene respectively. However, it is important to notice that the most efficient case, would be a third case, where all states involved in the rISC process are degenerate (^{1}CT, ^{3}CT and ^{3}LE) with ΔE_{ST} equal to zero.

Hiroyoshi Naito and co-authors[65] also investigated the control of the optical ΔE_{ST} gap by changing the polarity of the environment. They used 1,2-bis(carbazol-9-yl)-4,5-dicyanobenzene (2CzPN) as emitter doped in mixed host 1,3-bis(9-carbazolyl)benzene and camphoric anhydride (CA), which is a polar inert molecule. By increasing the CA concentration the permittivity of the devices increased linearly up to 40%. Also they observed that the energy of the singlet states red-shifted by increasing the permittivity of the devices; however, the energy of the triplet states remained unchanged. Thus, by changing the concentration of the hosts they could minimize the ΔE_{ST} in the devices, which is expected to result in a reduction of the triplet exciton density and, consequently, reduce roll-off in device efficiency.

We further evaluate the environmental polarity change by studying DPTZ-DPTO$_2$ in a PEO matrix. PEO enables us to study polarity dependence in the solid state as it has a temperature dependent dielectric coefficient. At room temperature the dielectric constant of PEO is quoted as ε≈ 5. However, this polarity is measured at microwave frequencies[66] and at optical frequencies we observe that PEO has a similar polarity to toluene at room temperature (ε≈2.38) given by the energy position of the DPTZ-DPTO$_2$ emission. Furthermore, the glass transition temperature (Tg) of PEO is 220 K, which causes the dielectric constant to decrease as the temperature decreases.

Figure 7 shows how the delayed emission properties of 2,8-DPTZ-DPTO$_2$ in PEO change as a function of temperature, especially around Tg. As the temperature of the film approaches the Tg from above, the ^{1}CT energy of the molecule blue shifts. The emission then stabilizes when the PEO becomes rigid below Tg. Alongside this increase in ^{1}CT energy there is also an increase in the intensity of the emission before it reduces again at low temperatures. Energetically this relates to the ^{1}CT energy level shifting from below the ^{3}LE state, passing through resonance at 220 K and then increasing further and stabilizing above the ^{3}LE state. The shift in the ^{1}CT energy onset is 100 meV from 2.50 to 2.60 eV bringing the states into resonance at 200 K and then out of resonance with the ^{3}LE state. The exchange energy between ^{1}CT and ^{3}CT in 2,8-DPTZ-DPTO$_2$ is small given its near perfect orthogonal D–A–D structure, even in a very low polarity medium[28]. Thus, throughout the thermal range used here ^{1}CT and ^{3}CT states will remain nearly isoenergetic. These measurements show that ^{1}CT emission is maximized when the gap between the CT states and the local triplet state (of the donor in this case) is minimized and that rISC and TADF depend critically on these energy gaps. Note that DF increases as the TADF emitter is cooled, showing that the energy gap between ^{1}CT and ^{3}LE plays the dominant role here. This has been nicely modelled recently by *Gibson and Penfold*[41].

This means that a molecule can be tuned from a bad TADF emitter into a good TADF emitter simply through changing the polarity of its host. This 'host tuning' was also demonstrated using a blue D-A-D TADF emitter[10], 2,7-bis(9,9-dimethyl-acridin-10-yl)-9,9-dimethylthioxanthene-*S,S*-dioxide (DDMA-TXO$_2$), where a polar host material tuned the ^{1}CT-^{3}LE gap from 150 meV in a non-polar host (zeonex) to 10 meV in polar DPEPO (Bis[2-(di- (phenyl)phosphino)-phenyl]ether oxide) (**Figure 8a**),

resulting in blue TADF devices with EQE values higher than 20%. The EQE *versus* brightness curve together with the chemical structure of the emitter and the device structure scheme is shown in **Figure 8b**. This shows that the host that is used in a TADF device plays just as critical a role as the TADF molecule itself in achieving high device performance.

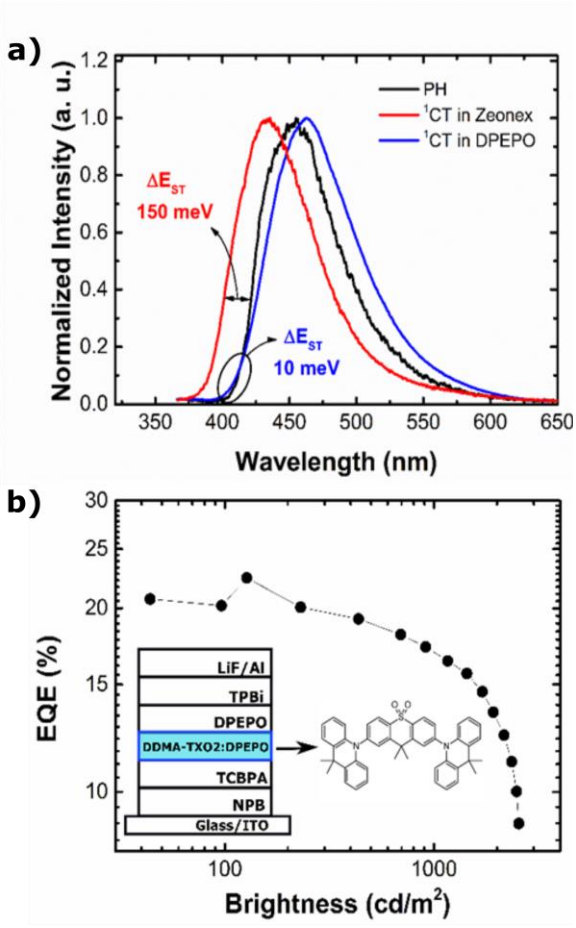

Figure 8 a) Singlet emission spectra (^{1}CT) of DDMA-TXO2 in zeonex and DPEPO hosts and phosphorescence spectra (PH). B) E.Q.E. versus current density of DDMA-TXO2:DPEPO device. Inset graph shows the device structure and the chemical structure of the emitter. Figure adapted from reference [10].

7. Control of conformation by energy excitation

The conformation of the D-A in the CT molecules can be affected by external factors, such as excitation energy, which also affects ΔE_{ST}. We identified dual CT emission in the emitter 2,7-bis(1-methylphenothiazin-10-yl)-9,9dimethylthioxanthene-*S,S*-dioxide (DMePT-TXO$_2$)[67], which has phenothiazine type donors, see chemical structure on inset of **Fig. 9a**. The axial and equatorial conformation can be controlled by the polarity of the environment as demonstrated by 3,7-DPTZ-DBTO$_2$ in section 5, and by the excitation energy. For the low polarity environment (MCH solution) and low excitation energy, 3.68 eV (337 nm), the emission of DMePT-TXO$_2$ shows contribution from: the axial-axial conformation ($CT_{ax\text{-}ax}$), which has strong locally excited state character and consequently shows weak solvatochromism; and the axial-equatorial conformation, $CT_{ax\text{-}eq}$, which shows strong solvatochromism. However, for higher energy excitation, 3.93 eV (316 nm), the relative intensity between the peaks changes significantly and the $CT_{ax\text{-}eq}$ contribution is enhanced and becomes the dominant emission. **Figure 9a** shows how the maximum intensity of each CT state in MCH solvent depends on the excitation energy. As can be seen, the emission which comes from the axial-axial conformation, $CT_{ax\text{-}ax}$, does not depend strongly on the excitation energy. However, the emission which comes from the axial-equatorial conformation, $CT_{ax\text{-}eq}$, is enhanced when the excitation occurs in the absorption peak of the A and D units (see full lines in **Fig.9a**). When the molecules are excited at lower energy, i.e., at the edge of the absorption spectrum, both states emit equally and weakly. Thus, higher excitation energy, with a high degree of excess energy, leads to the predominant formation of the $CT_{ax\text{-}eq}$ excited state, and we propose that the excess energy may enable molecular rearrangement from the ax-ax to the ax-eq conformation. The dual CT emission was also observed in zeonex matrix, a low polarity solid environment, but, contrary to the result in MCH, the ratio of the intensity of the two CT states is not dependent on the excitation energy (**Fig.9b**). This can be attributed to the fact that in solid state, the molecules are confined and are not free to re-orient as in solution.

The excitation energy also highlights different features in the triplet states. With excitation of 3.49 eV (355 nm) **Figure 9c**, the PH spectrum shows an interesting feature. As the time delay increases, an emission on the blue edge of the spectra grows in. This PH emission on the blue edge is assigned as the PH from the axial conformation, $^3LE_{ax}$, which acts as an effective loss pathway in the emission of this molecule. This higher energy triplet state does not couple with the $^1CT_{eq}$ state, which is the emission that dominates the prompt emission, preventing the TADF mechanism from occurring and giving rise to PH at RT. However, for excitation of 4.66 eV (266 nm) **Figure 9d**, the PH shows a different feature. A PH emission from the A units is also observed, which becomes the dominant triplet emission at later time delays. This strong triplet emission arises from the strong absorption of the A units at 266 nm (see **Fig. 9a**). The $^3LE_{ax}$ state thus is an energy sink in the DMePT-TXO$_2$ system, as has also been observed in other molecules where phenothiazine is in an axial conformation[49].

8. Conclusion

In conclusion, this review summarises the significant developments in the design and control of TADF molecules considering the spin-vibronic coupling mechanism. It highlights that even the earliest stage of choosing the donor and acceptor for the final molecule can have a significant effect on the final device performance. The main goal is to synthesise a CT molecule where ^{1}CT, ^{3}CT and ^{3}LE are all isoenergetic. From our development of TAT-3DBTO$_2$ we also now start to understand the benefit of having near degenerate multiple excited states which greatly enhance fluorescence quantum yield whilst maintaining a rISC rate > 10^7 s^{-1}, which is highly significant as it is a faster triplet harvesting rate than an Ir organometallic

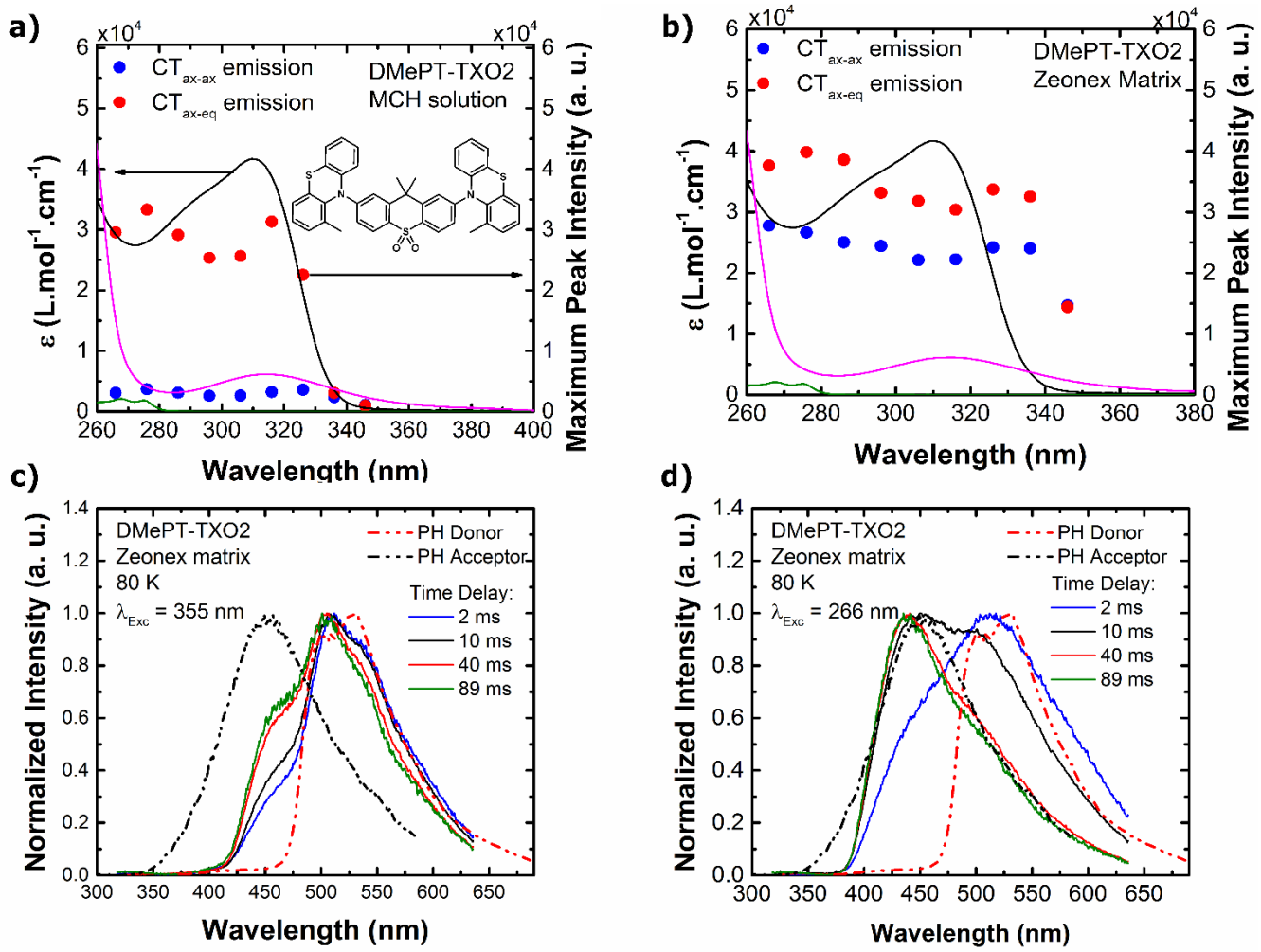

Figure 9 Maximum peak intensity of CT axial-axial emission (blue dot) and CT axial-equatorial emission (red dot) of DMePT-TXO2 in a) methylcyclohexane (MCH) solution and b) zeonex matrix at different energy excitations. Full lines show the extinction coefficient of DMePT-TXO$_2$ as well as its donor and acceptor units. c) Time resolved normalized emission spectra of DMePT-TXO$_2$ in the phosphorescence emission region for excitation at c) 355 nm and d) 266 nm at 80 K. The PH spectra of the donor and acceptor units are also shown for comparison. Figures adapted from reference [67].

complex! Flexible molecules due to their nature add an unpredictable element into the design stage, although this may not always be undesirable. We have considered here the specific case of phenothiazine and how in a series of high performing TADF molecules it has been identified to be the cause of two different emissive species. In the cases presented here it has a deleterious effect on the final TADF performance of the molecule. Replacing the phenothiazine with a different molecule will help avoid such problems. Furthermore, for any TADF molecules the polarity of the host can be used to tune the emissive and rISC properties of a molecule, turning a poor TADF emitter into one with high performance. This brings back some control to the designer and gives an extra direction of modification in the fabrication of OLEDs. Although, in contrast it may provide the added difficulty of matching the guest to the correct polarity host, whilst also maintaining beneficial charge balance and injection. Finally, we finish with an introduction into how excitation energy can have a significant effect on the ratio of the two emissive states in a phenothiazine-based D-A-D emitter. This provides an interesting insight into how conformation of a molecule can be the most crucial aspect that dominates its photophysics.

Acknowledgements

P. L. dos Santos thanks CAPES Foundation, Ministry of Education of Brazil, Science Without Borders Program for a PhD studentship, Proc. 12027/13-8. M. K. Etherington thanks the EU's Horizon 2020 for funding the PHEBE project under grant No. 641725. APM thanks the EPSRC (EP/L02621X/1) for funding.

References

1 F. Perrin, *Ann. Phys.*, 1929, **12**, 169–275.
2 G. N. Lewis, D. Lipkin and T. T. Magel, *J. Am. Chem. Soc.*, 1941, **63**, 3005–3018.
3 C. A. Parker and C. G. Hatchard, *Trans. Faraday Soc.*, 1961, **57**, 1894.
4 A. R. Horrocks and F. Wilkinson, 1968, **273**, 257–273.
5 F. Wilkinson and A. R. Horrocks, 1968, 116–153.
6 M. N. Berberan-Santos and J. M. M. Garcia, *J. Am. Chem. Soc.*, 1996, **7863**, 9391–9394.

7 C. Baleizão and M. N. Berberan-Santos, *Ann. N. Y. Acad. Sci.*, 2008, **1130**, 224–234.
8 A. Endo, M. Ogasawara, A. Takahashi, D. Yokoyama, Y. Kato and C. Adachi, *Adv. Mater.*, 2009, **21**, 4802–4806.
9 H. Uoyama, K. Goushi, K. Shizu, H. Nomura and C. Adachi, *Nature*, 2012, **492**, 234–8.
10 P. L. dos Santos, J. S. Ward, M. R. Bryce and A. P. Monkman, *J. Phys. Chem. Lett.*, 2016, 3341–3346.
11 C. W. Lee and J. Y. Lee, *ACS Appl. Mater. Interfaces*, 2015, **7**, 2899–2904.
12 T. Miwa, S. Kubo, K. Shizu, T. Komino, C. Adachi and H. Kaji, *Sci. Rep.*, 2017, **7**, 284.
13 D. de S. Pereira, P. L. dos Santos, J. S. Ward, P. Data, M. Okazaki, Y. Takeda, S. Minakata, M. R. Bryce and A. P. Monkman, *Sci. Rep.*, 2017, **7**, 6234.
14 F. B. Dias, K. N. Bourdakos, V. Jankus, K. C. Moss, K. T. Kamtekar, V. Bhalla, J. Santos, M. R. Bryce and A. P. Monkman, *Adv. Mater.*, 2013, **25**, 3707–3714.
15 D. de Sa Pereira, P. Data and A. P. Monkman, *Disp. Imaging*, 2017, **2**, 323–337.
16 Y. Luo and H. Aziz, *Adv. Funct. Mater.*, 2010, **20**, 1285–1293.
17 Z. Wu, L. Yu, X. Zhou, Q. Guo, J. Luo, X. Qiao, D. Yang, J. Chen, C. Yang and D. Ma, *Adv. Opt. Mater.*, 2016, **4**, 1067–1074.
18 S. Sinha and A. P. Monkman, *Appl. Phys. Lett.*, 2003, **82**, 4651–4653.
19 D. Y. Kondakov, *J. Appl. Phys.*, 2007, **102**.
20 A. P. Monkman, *ISRN Mater. Sci.*, 2013, **2013**, 670130.
21 S. Reindl and A. Penzkofer, *Chem. Phys.*, 1996, **211**, 431–439.
22 J. M. Larkin, W. R. Donaldson, T. H. Foster and R. S. Knox, *Chem. Phys.*, 1999, **244**, 319–330.
23 D. Hu, L. Yao, B. Yang and Y. Ma, *Philos. Trans. R. Soc. A Math. Phys. Eng. Sci.*, 2015, **373**, 20140318–20140318.
24 C. Torres Ziegenbein, S. Fröbel, M. Glöß, R. S. Nobuyasu, P. Data, A. Monkman and P. Gilch, *ChemPhysChem*, 2017, **18**, 2305.
25 B. Minaev, G. Baryshnikov and H. Agren, *Phys. Chem. Chem. Phys.*, 2014, **16**, 1719–1758.
26 J. Gibson, A. Monkman and T. Penfold, *ChemPhysChem*, 2016, **17**, 2956–2961.
27 M. K. Etherington, J. Gibson, H. F. Higginbotham, T. J. Penfold and A. P. Monkman, *Nat. Commun.*, 2016, **7**, 13680.
28 F. B. Dias, J. Santos, D. Graves, P. Data, R. S. Nobuyasu, M. A. Fox, A. S. Batsanov, T. Palmeira, M. N. Berberan-Santos, M. R. Bryce and A. P. Monkman, *Adv. Sci.*, 2016, **3**, 1–10.
29 P. L. Santos, J. S. Ward, P. Data, A. S. Batsanov, M. R. Bryce, F. B. Dias and A. P. Monkman, *J. Mater. Chem. C*, 2016, **4**, 3815--3824.
30 M. C. Gather and S. Reineke, *J. Photon. Energy*, 2015, **5**, 57607.
31 T. Palmeira and M. N. Berberan-santos, 2017, **708**.
32 F. B. Dias, *Proc. Roy. Soc*, 2015, **373**, 20140447.
33 Z. R. Grabowski, K. Rotkiewicz and A. Siemiarczuk, *J. Lumin.*, 1979, **18**–**19**, 420–424.
34 F. B. Dias, S. Pollock, G. Hedley, L. O. Pålsson, A. Monkman, I. I. Perepichka, I. F. Perepichka, M. Tavasli and M. R. Bryce, *J. Phys. Chem. B*, 2006, **110**, 19329–19339.
35 B. T. Lim, S. Okajima, A. K. Chandra and E. C. Lim, *Chem. Phys. Lett.*, 1981, **79**, 22–27.
36 M. Aydemir, G. Haykır, F. Türksoy, S. Gümüş, F. B. Dias and A. P. Monkman, *Phys. Chem. Chem. Phys.*, 2015, **17**, 25572–25582.
37 P. L. dos Santos, J. S. Ward, D. G. Congrave, A. S. Batsanov, J. E. Stacey, T. J. Penfold, A. P. Monkman and M. R. Bryce, *Just Accept. Adv. Sci.*, 2018, 1–23.
38 R. Huang, J. Avó, T. Northey, E. Chaning-Pearce, P. L. dos Santos, J. S. Ward, P. Data, M. K. Etherington, M. A. Fox, T. J. Penfold, M. N. Berberan-Santos, J. C. C. Lima, M. R. Bryce and F. Dias, *J. Mater. Chem. C*, 2017.
39 R. S. Nobuyasu, Z. Ren, G. C. Griffiths, A. S. Batsanov, P. Data, S. Yan, A. P. Monkman, M. R. Bryce and F. B. Dias, *Adv. Opt. Mater.*, 2015.
40 T. Ogiwara, Y. Wakikawa and T. Ikoma, *J. Phys. Chem. A*, 2015, **119**, 3415–3418.
41 J. Gibson and T. J. Penfold, *Phys. Chem. Chem. Phys.*, 2017, **19**, 8428–8434.
42 Y. Olivier, M. Moral, L. Muccioli and J.-C. Sancho-García, *J. Mater. Chem. C*, 2017, **5**, 5718–5729.
43 J. Daub, R. Engl, J. Kurzawa, S. E. Miller, S. Schneider, A. Stockmann and M. R. Wasielewski, *J. Phys. Chem. A*, 2001, **105**, 5655–5665.
44 A. Stockmann, J. Kurzawa, N. Fritz, N. Acar, S. Schneider, J. Daub, R. Engl and T. Clark, *J. Phys. Chem. A*, 2002, **106**, 7958–7970.
45 N. Acar, J. Kurzawa, N. Fritz, A. Stockmann, C. Roman, S. Schneider and T. Clark, *J. Phys. Chem. A*, 2003, **107**, 9530–9541.
46 J.-P. Malrieu and B. Pullman, *Theor. Chim. Acta*, 1964, **2**, 293–301.
47 C. Bodea and I. Silberg, *Chim. Int. J. Chem.*, 1968, **66**, 321–460.
48 J. L. Coubeils and B. Pullman, *Theor. Chim. Acta*, 1972, **24**, 35–41.
49 M. K. Etherington, F. Franchello, J. Gibson, T. Northey, J. Santos, J. S. Ward, H. F. Higginbotham, P. Data, A. Kurowska, P. L. Dos Santos, D. R. Graves, A. S. Batsanov, F. B. Dias, M. R. Bryce, T. J. Penfold and A. P. Monkman, *Nat. Commun.*, 2017, **8**, 14987.
50 M. Okazaki, Y. Takeda, P. Data, P. Pander, H. Higginbotham, A. P. Monkman and S. Minakata, *Chem. Sci.*, 2017, **8**, 2677–2686.
51 H. Tanaka, K. Shizu, H. Nakanotani and C. Adachi, *J. Phys. Chem. C*, 2014, **118**, 15985–15994.
52 K. Wang, C. J. Zheng, W. Liu, K. Liang, Y. Z. Shi, S. L. Tao, C. S. Lee, X. M. Ou and X. H. Zhang, *Adv. Mater.*, 2017, **29**, 1–9.
53 Q. Zhang, B. Li, S. Huang, H. Nomura, H. Tanaka and C. Adachi, *Nat. Photonics*, 2014, **8**, 1–7.
54 H. F. Higginbotham, C.-L. Yi, A. P. Monkman and K.-T. Wong, *J. Phys. Chem. C*, 2018, acs.jpcc.8b01579.
55 P. L. dos Santos, J. S. Ward, P. Data, A. Batsanov, M. R. Bryce, F. Dias and A. P. Monkman, *J. Mater. Chem. C*, 2016, **4**, 3815–3824.
56 J.-P. Malrieu and B. Pullman, *Theor. Chim. Acta*, 1964, **2**, 302–314.
57 Z. Aizenshtat, E. Klein, H. Weiler-Feilchenfeld and E. D. Bergmann, *Isr. J. Chem.*, 1972, **10**, 753–763.
58 T. Matulaitis, P. Imbrasas, N. A. Kukhta, P. Baronas, T. Bučiūnas, D. Banevičius, K. Kazlauskas, J. V. Gražulevičius and S. Juršėnas, *J. Phys. Chem. C*, 2017, acs.jpcc.7b08034.
59 J. S. Ward, R. S. Nobuyasu, A. S. Batsanov, P. Data, A. P.

Monkman, F. B. Dias and M. R. Bryce, *Chem. Commun.*, 2016, **52**, 3–6.
60 Y.-J. Lien, T.-C. Lin, C.-C. Yang, Y.-C. Chiang, C.-H. Chang, S.-H. Liu, Y.-T. Chen, G.-H. Lee, P.-T. Chou, C.-W. Lu and Y. Chi, *ACS Appl. Mater. Interfaces*, 2017, **9**, 27090–27101.
61 H. Tanaka, K. Shizu, H. Miyazaki and C. Adachi, *Chem. Commun.*, 2012, **48**, 11392.
62 M. Aydemir, S. Xu, C. Chen, M. R. Bryce, Z. Chi and A. P. Monkman, *J. Phys. Chem. C*, 2017, **121**, 17764–17772.
63 B. Xu, Y. Mu, Z. Mao, Z. Xie, H. Wu, Y. Zhang, C. Jin, Z. Chi, S. Liu, J. Xu, Y.-C. Wu, P.-Y. Lu, A. Lien and M. R. Bryce, *Chem. Sci.*, 2016, **7**, 2201–2206.
64 S. Xu, T. Liu, Y. Mu, Y. F. Wang, Z. Chi, C. C. Lo, S. Liu, Y. Zhang, A. Lien and J. Xu, *Angew. Chemie - Int. Ed.*, 2015, **54**, 874–878.
65 S. Haseyama, A. Niwa, T. Kobayashi, T. Nagase, K. Goushi, C. Adachi and H. Naito, *Nanoscale Res. Lett.*, 2017, **12**, 1–5.
66 C. Fanggao, G. A. Saunders, E. F. Lambson, R. N. Hampton, G. Carini, G. Di Marco and M. Lanza, *J. Polym. Sci. Part B Polym. Phys.*, 1996, **34**, 425–433.
67 P. L. dos Santos, J. S. Ward, A. S. Batsanov, M. R. Bryce and A. P. Monkman, *J. Phys. Chem. C*, 2017, **121**, 16462–16469.